Brillouin Light Scattering by Magnetic Quasivortices in Cavity Optomagnonics

A. Osada,[1,*] A. Gloppe,[1] R. Hisatomi,[1] A. Noguchi,[1] R. Yamazaki,[1] M. Nomura,[2] Y. Nakamura,[1,3] and K. Usami[1,†]
[1]*Research Center for Advanced Science and Technology (RCAST), The University of Tokyo, Meguro-ku, Tokyo 153-8904, Japan*
[2]*Institute of Industrial Science (IIS), The University of Tokyo, Meguro-ku, Tokyo 153-8505, Japan*
[3]*Center for Emergent Matter Science (CEMS), RIKEN, Wako, Saitama 351-0198, Japan*

(Received 25 November 2017; published 30 March 2018)

A ferromagnetic sphere can support optical vortices in the form of whispering gallery modes and magnetic quasivortices in the form of magnetostatic modes with nontrivial spin textures. These vortices can be characterized by their orbital angular momenta. We experimentally investigate Brillouin scattering of photons in the whispering gallery modes by magnons in the magnetostatic modes, zeroing in on the exchange of the orbital angular momenta between the optical vortices and magnetic quasivortices. We find that the conservation of the orbital angular momentum results in different nonreciprocal behavior in the Brillouin light scattering. New avenues for chiral optics and optospintronics can be opened up by taking the orbital angular momenta as a new degree of freedom for cavity optomagnonics.

DOI: 10.1103/PhysRevLett.120.133602

Vortexlike excitations, which can be characterized by a topological charge or an orbital angular momentum (OAM), have been intensively studied in the past decades and are still a hot topic in both scientific and technological contexts. An optical vortex [1], for instance, is utilized for manipulating microparticles [2] and atoms [3,4], for OAM multiplexing in telecommunication [5], and encoding quantum information [6,7]. In condensed matter research, spin textures in spin systems, that is, magnetic vortices, have been and still are a focus in the context of magnetic domain walls [8] as well as magnetic Skyrmions [9], e.g., in the scope of using them for information storage.

The interaction between optical vortices and magnetic vortices is expected to show novel physics owing to the exchange of the OAM. A system providing a platform for such an interaction is a ferromagnetic sphere, supporting both optical whispering gallery modes (WGMs) [10] for photons and magnetostatic (Walker) modes [11,12] for magnons. We refer to the WGMs as "optical vortices" and the Walker modes as "magnetic quasivortices," where the prefix "quasi" emphasizes the fact that (1) a magnon is a quasiparticle with a finite lifetime and (2) the OAM for the Walker mode is approximately well defined if the Zeeman energy is dominant over the axial-symmetry-broken dipolar interaction [13].

An emerging field called cavity optomagnonics, aiming at enhancing magnon-induced Brillouin light scattering [14–20], takes place in such a platform. Up until now, the magnetostatic modes used in the experiments of cavity optomagnonics [14–17] remain limited to the uniform precession mode, or the Kittel mode, having no OAM, which has also been utilized for experiments on the circuit quantum magnonics [21–26], as well as for the coherent conversion between microwave and optical photons [27].

In this Letter, the Brillouin light scattering hosted in a ferromagnetic sphere is experimentally investigated with a special emphasis on the magnetostatic modes involving magnetic quasivortices. The experiments reveal that the scattering is either nonreciprocal or reciprocal depending on the OAM of the magnons. We analyze the results with the theory developed in [13], which analyzes the behaviors of Brillouin scattering of WGMs by Walker modes based on the orbital and spin angular momentum conservation, and find reasonable agreements. The OAM can thus be considered as a new degree of freedom in cavity optomagnonics, providing a new approach to chiral quantum optics [28] and topological photonics [29,30].

Let us first describe the characteristics of the Walker modes and the WGMs in terms of OAM. Henceforth, we shall suppose that the symmetry axis is the z axis, along which a static magnetic field is applied, perpendicular to the plane of the WGM orbit. The Walker modes are nominally labeled by three indices (n, m_{mag}, r) [11,12], where the second index m_{mag} is the most relevant one. This index is related to the OAM $\mathcal{L}_z^{(m_{\mathrm{mag}})}$, defined by the winding number of the spin texture, as $\mathcal{L}_z^{(m_{\mathrm{mag}})} \simeq -(m_{\mathrm{mag}} - 1)$ under proper approximations [13], while n and r are related to the profiles along polar and radial directions, respectively.

In Fig. 1(a), the distributions of the magnetization component perpendicular to the symmetry axis for some Walker modes are exemplified [11–13]. For these four modes labeled by (1,1,0), $(3, \bar{1}, 1)$, (3,1,1), and (4,0,1), the orbital angular momenta are $\mathcal{L}_z^{(1)} = 0$, $\mathcal{L}_z^{(-1)} = 2$, $\mathcal{L}_z^{(1)} = 0$, and $\mathcal{L}_z^{(0)} = 1$, respectively. It is apparent that the modes with nonzero OAM exhibit topologically nontrivial spin textures, that is, "magnetic quasivortices."

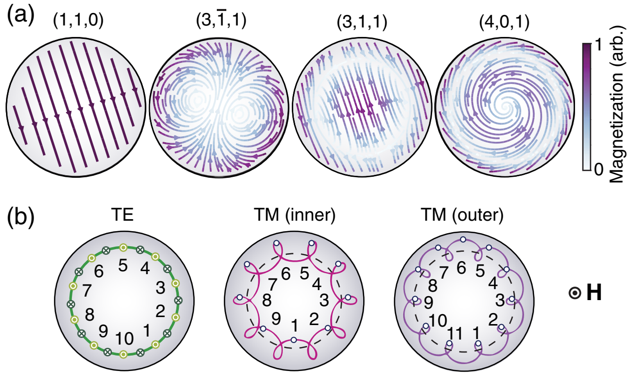

FIG. 1. (a) Transverse magnetization distributions of (1,1,0), $(3,\bar{1},1)$, (3,1,1), and (4,0,1) Walker modes in the equatorial plane. (b) Schematic representations of the heads of the electric fields of TE and TM WGMs on the equatorial plane. These illustrate the difference of OAM for the TE WGM, the inner component of TM WGM, and the outer component of the TM WGM for the case of $m = 10$. The hollow circles locate points where the field vectors direct upward for the ease of counting the numbers of the phase rotations in Cartesian coordinates.

Next we consider the OAM of the WGM. Let the optical field orbiting counterclockwise (CCW) be decomposed into three components based on their spins along the symmetry axis z. A transverse-electric (TE) WGM, whose direction of the field is parallel to the z axis and schematically shown in the left panel of Fig. 1(b), is π polarized. If the TE WGM has the azimuthal mode index of m_{TE}, the light field oscillates m_{TE} times in the CCW round-trip and therefore the OAM reads as $\mathcal{L}_z^{(\mathrm{CCW,TE},m_{\mathrm{TE}})} = m_{\mathrm{TE}}$. On the other hand, a transverse-magnetic (TM) WGM has the polarization in the plane of the WGM orbit which is decomposed into σ^+ and σ^- components. The orbital angular momenta are different for these two components. The situation is shown in the center and right panels of Fig. 1(b). The trajectories of the head of the polarization vector for each electric field are shown. For the ease of counting the numbers of rotations of the head, hollow circles indicate positions around which the electric field directs upward. When the mode index is 10, the orbital angular momentum reads 10, 9, and 11 for the TE, inner TM, and outer TM components, respectively [13]. Here we call the polarization component giving the smaller (larger) number of phase rotation the inner (outer) component, since it actually comes from the inner (outer) region of the WGM distribution as a result of the spin-Hall effect of light [31,32]. The origin of such an effect is the transversality of the electromagnetic field, which couples spin (polarization) and orbital degrees of freedom of light [33]. Consequently, the OAM is not a good quantum number for the TM WGM and is given by $\mathcal{L}_z^{(\mathrm{CCW,TM}+,m_{\mathrm{TM}})} = m_{\mathrm{TM}} - 1$ for the inner component and $\mathcal{L}_z^{(\mathrm{CCW,TM}-,m_{\mathrm{TM}})} = m_{\mathrm{TM}} + 1$ for the outer component, respectively. Here the "TM±" in the superscript refers to the OAM accompanying the $\sigma^{\pm}$-polarized

TABLE I. List of orbital angular momenta exhibited by each polarization component of whispering gallery modes analyzed in Ref. [13].

Direction	$\mathcal{L}_z^{(\mathrm{Direction,TE},m_{\mathrm{TE}})}$	$\mathcal{L}_z^{(\mathrm{Direction,TM}\pm,m_{\mathrm{TM}})}$
CW	$-m_{\mathrm{TE}}$	$-(m_{\mathrm{TM}} \pm 1)$
CCW	m_{TE}	$m_{\mathrm{TM}} \mp 1$

component. Note that the total angular momentum defined by the sum of the OAM and spin angular momentum for each of these two components is the same and a good quantum number.

For the clockwise (CW) orbit, on the other hand, the orbital angular momenta of these inner and outer components of the TM WGM are given with the proper sign inversion, that is, $\mathcal{L}_z^{(\mathrm{CW,TM}+,m_{\mathrm{TM}})} = -(m_{\mathrm{TM}} + 1)$ and $\mathcal{L}_z^{(\mathrm{CW,TM}-,m_{\mathrm{TM}})} = -(m_{\mathrm{TM}} - 1)$. Note that the OAM of the TE WGM orbiting clockwise is straightforwardly given by $\mathcal{L}_z^{(\mathrm{CW,TE},m_{\mathrm{TE}})} = -m_{\mathrm{TE}}$. These observations, which are detailed in Ref. [13], are summarized in Table I.

We experimentally investigate how these orbital angular momenta of the magnons and the photons are exchanged in a ferromagnetic sphere. The sample under consideration is a yttrium iron garnet (YIG) sphere with a diameter of 1 mm. We focus on the Brillouin scattering induced by the magnetic quasivortices with $\mathcal{L}_z^{(m_{\mathrm{mag}})} = 0, 1, 2$, which include the (1,1,0), (3,1,1), (4,0,1), and $(3,\bar{1},1)$ Walker modes.

The experimental setup is schematically shown in Fig. 2. Laser light with a wavelength of 1550 nm is coupled to WGMs in the YIG sphere via a silicon prism. The quality factor of WGMs in the YIG sphere is around 10^5. Whether

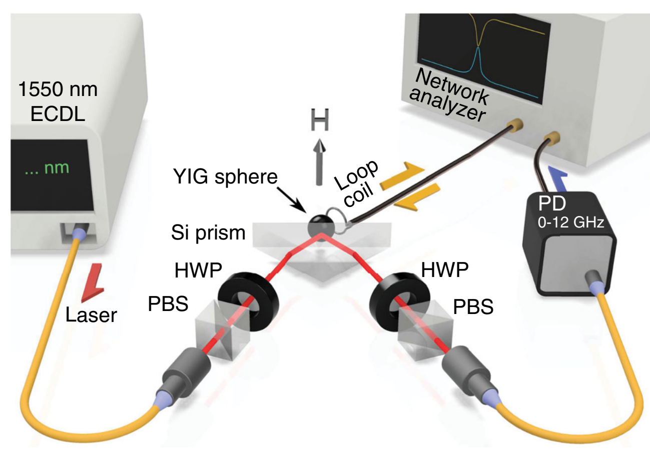

FIG. 2. Experimental setup for observing the Brillouin scattering. External-cavity diode laser (ECDL) supplies the laser light of 1550-nm wavelength. Its polarization is defined by a PBS and a HWP to be coupled to a particular family of the YIG sphere WGM by the intercession of the silicon prism. Microwaves from a network analyzer excite magnons via a loop coil. Scattered and unscattered light interfere through a HWP and a PBS, and the beat signal is detected by a high-speed PD and analyzed by the network analyzer.

the TE or the TM family of WGMs is coupled depends on the linear polarization before the prism, which is determined by a polarization beam splitter (PBS) and a half wave plate (HWP). The input polarization and the frequency of the laser light is tuned to couple into a certain TM WGM on resonance. The static magnetic field around 0.25 T, giving a Kittel mode frequency of 7.1 GHz, saturates the magnetization of the sample in the direction perpendicular to the plane of the WGM orbit. Microwaves are sent from a network analyzer to a loop coil and excite magnons in a specific Walker mode. The photons in the TM WGM are then scattered simultaneously, creating (annihilating) a magnon and generating a Stokes-sideband (anti-Stokes-sideband) photon into the TE WGM [13]. A PBS and HWP after the prism make the scattered and unscattered photons interfere. The beat signal at the magnon frequency is detected by a high-speed photodetector (PD) and sent back to the network analyzer.

The microwave reflection spectrum is plotted in Fig. 3(a) with the indices of the identified Walker modes next to the

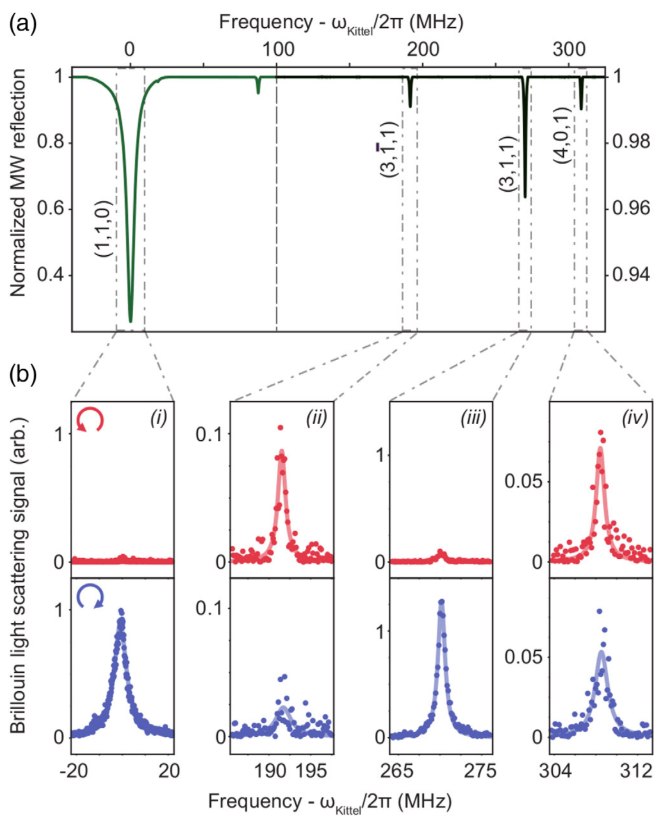

FIG. 3. (a) Normalized microwave (MW) reflection spectrum with the mode indices assigned to the Walker modes of our interest. Along the horizontal axis, the relative frequency to the Kittel mode frequency $\omega_{\mathrm{Kittel}}/2\pi$ is used. Note that the spectra below (green, left axis) and above (black, right axis) 100 MHz are separately scaled. (b) The signals of the Brillouin scattering of the CCW (red) and the CW (blue) WGMs by (i) (1,1,0), (ii) $(3,\bar{1},1)$, (iii) (3,1,1), and (iv) (4,0,1) Walker modes. Solid lines are Lorentzian fittings to the data as a guide to the eye.

observed dips [34]. Spectra in Fig. 3(b) are the observed signals of the scattered light generated by each of the four Walker modes for CCW (red) and CW orbits (blue). For the Walker modes possessing no OAM, that is, (1,1,0) and (3,1,1) modes, the Brillouin scattering tends to occur more prominently for the CW orbit than that for the CCW orbit. As for the (4,0,1) mode, which has the orbital angular momentum $\mathcal{L}_z^{(0)} = 1$, the signal strengths of the Brillouin scattering for the CW orbit and that for the CCW orbit are more or less equal. As for the $(3,\bar{1},1)$ mode, where the OAM reads $\mathcal{L}_z^{(-1)} = 2$, however, the Brillouin scattering tends to occur more prominently for the CCW orbit than for the CW orbit.

These results can be explained by the following selection rule in the Brillouin light scattering process [13]. First, the light is supposed to be injected into the TM WGM with the mode index m_{TM} orbiting CCW. According to the angular momentum conservation, the photons in the TM WGM would be scattered into the TE WGM with the mode index m_{TE}, which must satisfy

$$\mathcal{L}_z^{(\mathrm{CCW,TE},m_{\mathrm{TE}})} - \mathcal{L}_z^{(\mathrm{CCW,TM+},m_{\mathrm{TM}})} - \mathcal{L}_z^{(m_{\mathrm{mag}})} = 0,$$

which leads to the selection rule

$$m_{\mathrm{TE}} = m_{\mathrm{TM}} - m_{\mathrm{mag}} \tag{1}$$

in the anti-Stokes scattering process associated with the inner component of the input TM WGM, and

$$\mathcal{L}_z^{(\mathrm{CCW,TE},m_{\mathrm{TE}})} - \mathcal{L}_z^{(\mathrm{CCW,TM-},m_{\mathrm{TM}})} + \mathcal{L}_z^{(m_{\mathrm{mag}})} = 0,$$
$$m_{\mathrm{TE}} = m_{\mathrm{TM}} + m_{\mathrm{mag}} \tag{2}$$

in the Stokes scattering process associated with the outer component of the input TM WGM. On the contrary, if the light is injected into the CW-orbiting TM WGM, the orbital angular momentum conservation and the selection rules become

$$\mathcal{L}_z^{(\mathrm{CW,TE},m_{\mathrm{TE}})} - \mathcal{L}_z^{(\mathrm{CW,TM+},m_{\mathrm{TM}})} - \mathcal{L}_z^{(m_{\mathrm{mag}})} = 0,$$
$$m_{\mathrm{TE}} = m_{\mathrm{TM}} + m_{\mathrm{mag}} \tag{3}$$

in the anti-Stokes scattering process, which is now associated with the outer component of the input TM WGM, and

$$\mathcal{L}_z^{(\mathrm{CW,TE},m_{\mathrm{TE}})} - \mathcal{L}_z^{(\mathrm{CW,TM-},m_{\mathrm{TM}})} + \mathcal{L}_z^{(m_{\mathrm{mag}})} = 0,$$
$$m_{\mathrm{TE}} = m_{\mathrm{TM}} - m_{\mathrm{mag}} \tag{4}$$

in the Stokes scattering process associated with the inner component of the input TM WGM.

Now, let us see how the selection rule given above and the spectral properties of the WGMs dictates the Brillouin scattering process. Figures 4(a)–4(c) show schematically the densities of states of the TM (purple) and the TE (green) WGMs. Here, for a given azimuthal mode index m_{TM}, the resonance frequencies of the TM and the TE WGMs are different due to the geometric birefringence (GB) [40–42] by ~32 GHz, which is adopted from the experimental value, as well as the free spectral range (FSR) of ~40 GHz. Two sets of the WGMs are depicted (top and bottom), one for the inner component [$\sigma_+(\sigma_-)$ component for the CCW (CW) orbit] and the other for the outer component [$\sigma_-(\sigma_+)$ component for the CCW (CW) orbit].

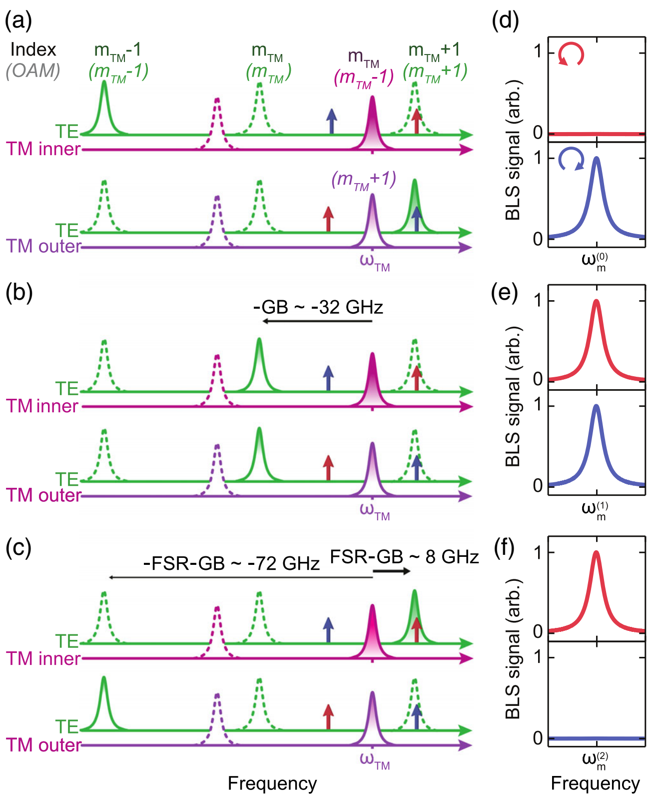

FIG. 4. (a)–(c) Densities of states of the relevant WGMs (highlighted, otherwise dotted) for the magnon-induced Brillouin light scattering. Here we assume that the input mode is TM with an azimuthal index of m_{TM} at a frequency of $\omega_{\mathrm{TM}}/2\pi$. The TM modes are split into inner (pink) and outer (purple) components, with the OAM of $m_{\mathrm{TM}}-1$ and $m_{\mathrm{TM}}+1$, respectively. Because of the GB, in our experiment, the TE modes (green) are shifted by ~ -32 GHz in comparison to the TM modes. Two adjacent modes of the same polarization are separated by the FSR ~ 40 GHz. (a)–(c) Situations for the considered Walker mode OAM of $\mathcal{L}_z^{(1)}=0$, $\mathcal{L}_z^{(0)}=1$, and $\mathcal{L}_z^{(-1)}=2$, respectively. The scattered photons are depicted by blue and red arrows, representing, respectively, clockwise and counterclockwise input orbits. (d)–(f) Theoretically predicted nonreciprocal or reciprocal behavior of the Brillouin light scattering (BLS) for the CCW (red) and the CW orbit (blue) inputs, respectively, for cases (a)–(c). The symbol $\omega_m^{(i)}$ represents the Walker mode frequency where i designates the OAM.

First, we consider the Walker modes with the OAM $\mathcal{L}_z^{(1)}=0$, that is, (1,1,0) and (3,1,1) modes. In this case, we have the selection rules Eqs. (1)–(4) with $m_{\mathrm{mag}}=1$. The relevant TE WGMs specified by the selection rule are highlighted (otherwise dotted) in Fig. 4(a). In Fig. 4(a), the expected frequencies of the TE photons to be created are indicated by blue and red upright arrows for the CW and the CCW orbits, respectively. We see that whether the Stokes scattering or the anti-Stokes scattering occurs out of the inner or outer components of the TM WGM depends on the direction of the WGM orbit. As for the inner component (pink), the scattered light for both the CW and the CCW orbits are far detuned from the relevant TE WGM specified by the selection rule by ~FSR + GB = 72 GHz [cf. the arrow in Fig. 4(c)]. On the other hand, for the outer component (purple), the scattered light is almost resonant for the CW orbit and off resonant for the CCW orbit. In Fig. 4(d), the theoretically predicted nonreciprocal behavior of the Brillouin scattering is schematically shown, where the blue and red curves are, respectively, for the CW and the CCW cases. This is in good agreement with the experimental results shown in Fig. 3(b) (i) and (iii).

The same argument applies for other cases. In Figs. 4(b) and 4(c), the relevant TE WGMs specified by the selection rules are highlighted (otherwise dotted) as in Fig. 4(a). For the (4,0,1) mode with the OAM $\mathcal{L}_z^{(0)}=1$, the selection rules becomes simply $m_{\mathrm{TE}}=m_{\mathrm{TM}}$, resulting in the absence of the nonreciprocity as indicated in Fig. 4(e). The observed reciprocity in Fig. 3(b) (iv) can thus be explained. Note here that the scattered light in this case is off resonant by ~25 GHz from the relevant WGM both for the CW input and the CCW input. As for the Walker mode with the OAM $\mathcal{L}_z^{(-1)}=2$, such as the $(3,\bar{1},1)$ mode, the selection rules are exactly the same as for the modes with the OAM $\mathcal{L}_z^{(1)}=0$, but the roles of the CCW and the CW orbits are interchanged. This leads to the prediction of the nonreciprocal behavior depicted in Fig. 4(f), which is again in good agreement with the experimental result shown in Fig. 3(b) (ii).

Given the detuning from the resonant conditions, the numbers of excited magnons, and the observed signal strengths, the optomagnonic coupling constants involving (3,1,1), (4,0,1), and $(3,\bar{1},1)$ modes can be estimated to be 3, 12, and 2 times larger than that of the Kittel mode, respectively. The origin of these enhanced couplings is deduced to be the reduced mode volume of the Walker mode compared to the one of the Kittel mode (see the Supplemental Material of Refs. [15,20]), while the quantitative explanation requires further theoretical and numerical investigation.

In summary, we experimentally investigated the Brillouin light scattering within a ferromagnetic sphere and observed nontrivial nonreciprocal or reciprocal behavior of the Brillouin light scattering by the magnons with and without orbital angular momenta. We showed that the observed phenomena can be understood in terms of conservative exchange of the orbital angular momentum between the photons in whispering gallery modes and the magnons in the Walker mode. Nonreciprocity and topology are at the heart of the current research activities in photonics, spintronics, and magnonics. Our findings suggest that cavity optomagnonics embrace these two concepts and could thus be an alternative and attractive platform for further developing chiral and topological devices.

We are grateful to Y. Shikano, Y. Tabuchi, Y. Nakata, S. Ishino, G. Tatara, S. Iwamoto, J. Haigh, S. Sharma, Y. M. Blanter, and G. E. W. Bauer for fruitful discussions. This work was supported by JSPS KAKENHI (Grants No. 15H05461, No. 16F16364, No. 26220601, and No. 26600071), Murata Science Foundation, Inamori Foundation, and JST ERATO project (Grant No. JPMJER1601). A. G. is an overseas researcher under a Postdoctoral Fellowship of JSPS.

[*]Present address: Institute for Nano Quantum Information Electronics, The University of Tokyo, Meguro-ku, Tokyo 153-8505, Japan.
alto@iis.u-tokyo.ac.jp
[†]usami@qc.rcast.u-tokyo.ac.jp

[1] L. Allen, S. M. Barnett, and M. J. Padgett, *Optical Angular Momentum* (CRC Press, Boca Raton, FL, 2003).
[2] D. G. Grier, Nature (London) **424**, 21 (2003).
[3] D. Akamatsu and M. Kozuma, Phys. Rev. A **67**, 023803 (2003).
[4] M. F. Andersen, C. Ryu, P. Cladé, V. Natarajan, A. Vaziri, K. Helmerson, and W. D. Phillips, Phys. Rev. Lett. **97**, 170406 (2006).
[5] J. Wang, J.-Y. Yang, I. M. Fazal, N. Ahmed, Y. Yan, H. Huang, Y. Ren, Y. Yue, S. Dolinar, M. Tur, and A. E. Willner, Nat. Photonics **6**, 488 (2012).
[6] A. Mair, A. Vaziri, G. Weihs, and A. Zeilinger, Nature (London) **412**, 313 (2001).
[7] R. Inoue, T. Yonehara, Y. Miyamoto, M. Koashi, and M. Kozuma, Phys. Rev. Lett. **103**, 110503 (2009).
[8] A. Malozemoff and J. Slonczewski, *Magnetic Domain Walls in Bubble Materials* (Academic Press, New York, 1979).
[9] N. Nagaosa and Y. Tokura, Nat. Nanotechnol. **8**, 899 (2013).
[10] K. Vahala, Nature (London) **424**, 839 (2003).
[11] L. R. Walker, Phys. Rev. **105**, 390 (1957).
[12] P. C. Fletcher and R. O. Bell, J. Appl. Phys. **30**, 687 (1959).
[13] A. Osada, A. Gloppe, Y. Nakamura, and K. Usami, arXiv:1711.09321.
[14] J. A. Haigh, S. Langenfeld, N. J. Lambert, J. J. Baumberg, A. J. Ramsay, A. Nunnenkamp, and A. J. Ferguson, Phys. Rev. A **92**, 063845 (2015).
[15] A. Osada, R. Hisatomi, A. Noguchi, Y. Tabuchi, R. Yamazaki, K. Usami, M. Sadgrove, R. Yalla, M. Nomura, and Y. Nakamura, Phys. Rev. Lett. **116**, 223601 (2016).
[16] X. Zhang, N. Zhu, C.-L. Zou, and H. X. Tang, Phys. Rev. Lett. **117**, 123605 (2016).
[17] J. A. Haigh, A. Nunnenkamp, A. J. Ramsay, and A. J. Ferguson, Phys. Rev. Lett. **117**, 133602 (2016).
[18] S. V. Kusminskiy, H. X. Tang, and F. Marquardt, Phys. Rev. A **94**, 033821 (2016).
[19] T. Liu, X. Zhang, H. X. Tang, and M. E. Flatte, Phys. Rev. B **94**, 060405(R) (2016).
[20] S. Sharma, Y. M. Blanter, and G. E. W. Bauer, Phys. Rev. B **96**, 094412 (2017).
[21] Y. Tabuchi, S. Ishino, T. Ishikawa, R. Yamazaki, K. Usami, and Y. Nakamura, Phys. Rev. Lett. **113**, 083603 (2014).
[22] N. Kostylev, M. Goryachev, and M. E. Tobar, Appl. Phys. Lett. **108**, 062402 (2016).
[23] X. Zhang, C. Zou, L. Jiang, and H. X. Tang, J. Appl. Phys. **119**, 023905 (2016).
[24] L. Bai, M. Harder, Y. P. Chen, X. Fan, J. Q. Xiao, and C.-M. Hu, Phys. Rev. Lett. **114**, 227201 (2015).
[25] Y. Tabuchi, S. Ishino, A. Noguchi, T. Ishikawa, R. Yamazaki, K. Usami, and Y. Nakamura, Science **349**, 405 (2015).
[26] D. Lachance-Quirion, Y. Tabuchi, S. Ishino, A. Noguchi, T. Ishikawa, R. Yamazaki, and Y. Nakamura, Sci. Adv. **3**, e1603150 (2017).
[27] R. Hisatomi, A. Osada, Y. Tabuchi, T. Ishikawa, A. Noguchi, R. Yamazaki, K. Usami, and Y. Nakamura, Phys. Rev. B **93**, 174427 (2016).
[28] P. Lodahl, S. Mahmoodian, S. Stobbe, A. Rauschenbeutel, P. Schneeweiss, J. Volz, P. Pichler, and P. Zoller, Nature (London) **541**, 473 (2017).
[29] M. Hafezi and J. M. Taylor, Phys. Today **67**, No. 5, 68 (2014).
[30] L. Lu, J. D. Joannopoulos, and Marin Soljačić, Nat. Photonics **8**, 821 (2014).
[31] M. Onoda, S. Murakami, and N. Nagaosa, Phys. Rev. Lett. **93**, 083901 (2004).
[32] K. Y. Bliokh, D. Smirnova, and F. Nori, Science **348**, 1448 (2015).
[33] K. Y. Bliokh, F. J. Rodríguez-Fortuño, F. Nori, and A. V. Zayats, Nat. Photonics **9**, 796 (2015).
[34] See Supplemental Material at http://link.aps.org/supplemental/10.1103/PhysRevLett.120.133602 for the assignment of the mode indices for the observed Walker modes, which includes Refs. [35–39].
[35] J. E. Mercereau, J. Appl. Phys. **30**, S184 (1959).
[36] P. C. Fletcher, I. H. Solt, and R. Bell, Phys. Rev. **114**, 739 (1959).
[37] R. Plumier, Physica (Utrecht) **28**, 423 (1962).
[38] I. H. Solt and P. C. Fletcher, J. Appl. Phys. **31**, S100 (1960).
[39] V. L. Launets, M. M. Novitskas, and V. K. Shugurov, Radiophys. Quantum Electron. **14**, 734 (1971).
[40] S. Schiller and R. L. Byer, Opt. Lett. **16**, 1138 (1991).
[41] C. C. Lam, P. T. Leung, and K. Young, J. Opt. Soc. Am. B **9**, 1585 (1992).
[42] S. Schiller, Appl. Opt. **32**, 2181 (1993).